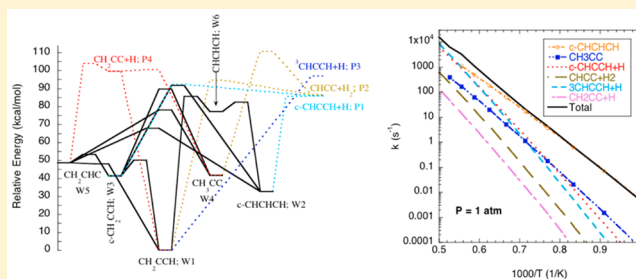


Kinetics of Propargyl Radical Dissociation

Stephen J. Klippenstein,[†] James A. Miller,^{*,†} and Ahren W. Jasper[‡][†]Chemical Sciences and Engineering Division, Argonne National Laboratory, Argonne, Illinois 60439, United States[‡]Combustion Research Facility, Sandia National Laboratories, Livermore, California 94551, United States

Supporting Information

ABSTRACT: Due to the prominent role of the propargyl radical for hydrocarbon growth within combustion environments, it is important to understand the kinetics of its formation and loss. The ab initio transition state theory-based master equation method is used to obtain theoretical kinetic predictions for the temperature and pressure dependence of the thermal decomposition of propargyl, which may be its primary loss channel under some conditions. The potential energy surface for the decomposition of propargyl is first mapped at a high level of theory with a combination of coupled cluster and multireference perturbation calculations. Variational transition state theory is then used to predict the microcanonical rate coefficients, which are subsequently implemented within the multiple-well multiple-channel master equation. A variety of energy transfer parameters are considered, and the sensitivity of the thermal rate predictions to these parameters is explored. The predictions for the thermal decomposition rate coefficient are found to be in good agreement with the limited experimental data. Modified Arrhenius representations of the rate constants are reported for utility in combustion modeling.



1. INTRODUCTION

The recombination of two propargyl (CH_2CCH) radicals is commonly found to provide the dominant route to formation of the first aromatic ring within combustion environments.^{1–5} For some conditions, the reaction of propargyl with other species, such as allyl or acetylene, may also play a role in ring formation. Related reactions of propargyl with polycyclic aromatic hydrocarbon radicals such as benzyl likely play a similarly important role in ring expansion.⁶

The importance of the propargyl radical to hydrocarbon growth in high-temperature environments is related to its exceptional thermal and chemical stability, which results in remarkably high concentrations in the steady-state environment of flames. Indeed, the concentration of propargyl radicals often rivals that of the major closed shell intermediates that are also central to the hydrocarbon growth process. This stability is partly due to the presence of two resonant electronic configurations for propargyl, where the radical electron is viewed as localized on either the CH_2 (head) or the CH (tail) end of the molecule. These resonant configurations imply a lower electronic energy and thus increased thermal stability. They also imply a lower chemical reactivity because the resonance must be broken prior to chemical bond formation at one of the radical sites. As a result, the entrance barriers for its addition reactions are generally greater than the usual case where neither of the radicals is a resonantly stabilized radical. Furthermore, the exothermicity of the addition process is reduced by the resonance stabilization energy of propargyl, which reduces the probability of both collisional stabilization and of further isomerizations.

There are, of course, many other similarly resonantly stabilized radicals in the combustion environment, such as allyl (CH_2CHCH_2) and $i\text{-C}_4\text{H}_3$ (CH_2CCCH). However, the role of such radicals is generally not nearly as significant as that of propargyl. The increased importance of the propargyl radical relative to other resonantly stabilized radicals is related to the difficulty of further dehydrogenation of propargyl.

Simple CH bond fission of a radical generally leads to a stable closed shell alkene or alkyne, with typical bond dissociation energies, D_0 , of about 35 kcal/mol (e.g., C_2H_3 and C_2H_5 have D_0 values of 34 and 35 kcal/mol, respectively). For resonantly stabilized radicals, the CH bond-fission still generally produces a closed shell molecule, but D_0 is generally increased by the resonance stabilization energy of the radical, which is typically about 10 to 20 kcal/mol. For example, for allyl and $i\text{-C}_4\text{H}_3$ (CH_2CCCH), the CH bond fission energies are 56 and 43 kcal/mol, respectively. Such bond dissociation energies are still small enough that thermal dissociation provides a rapid loss, resulting in modest steady-state concentrations. However, for propargyl, simple CH bond fission leads to either a triplet CHCCH diradical or a CH_2CC carbene, both of which are highly unstable due to an insufficiency of valence electrons. As a

Special Issue: 100 Years of Combustion Kinetics at Argonne: A Festschrift for Lawrence B. Harding, Joe V. Michael, and Albert F. Wagner

Received: February 3, 2015

Revised: April 10, 2015

Published: April 14, 2015



result, for propargyl, the CH fission energies are 96 and 99 kcal/mol for the head and tail fissions, respectively. Notably, phenyl and benzyl radicals, which are of similar importance to the hydrocarbon growth process as the propargyl radical, also exhibit a similar resistance to dehydrogenation with simple CH bond fission energies of 94 and 108 kcal/mol, respectively.⁷

Importantly, the resistance to further dehydrogenation also implies lower reactivity with O₂. Generally, the formation of HO₂, through either direct abstraction or an addition–elimination process, is the most important channel for the reaction of radicals with O₂, particularly at the higher temperatures of relevance to hydrocarbon growth. However, for propargyl this process is highly endothermic and thus has a greatly reduced rate constant. As a result, even though the propargyl radical is very stable, its thermal decomposition may still provide an important loss channel, and a proper delineation of propargyl's role in combustion chemistry requires accurate estimates for the temperature and pressure dependence of the decomposition rate constant. However, as a consequence of the present analysis, it appears that thermal dissociation is only a minor reaction channel for propargyl under most combustion conditions.

The only experimental measurement of the rate constant for the thermal decomposition of the propargyl radical appears to be that obtained in a shock tube study of 3-iodo-propyne, which covered temperatures ranging from 1400–2000 K and pressures ranging from 1.5–2.2 bar.⁸ Related experimental and theoretical studies of the photodissociation of propargyl,^{9–12} the reaction of CH(²Π) with acetylene,^{10,13–17} and of C(³P) with the vinyl radical^{10,18} have led to a detailed understanding of the mechanism for isomerization and decomposition on the C₃H₃ potential energy surface. Unfortunately, this mechanistic understanding has not been used to predict the temperature and pressure dependence of the thermal decomposition kinetics. The only theoretical predictions for the thermal decomposition of propargyl appear to be the hindered Gorin model calculations performed by Kiefer et al.¹⁹ as part of their shock-tube study of the dissociation of C₃H₄. The most closely related theoretical study was a prediction of the high-pressure-limit rate coefficient for the related recombination of H with ³CHCCH (which correlates with the dominant channel in photodissociation of propargyl) with CASPT2 (complete-active-space second-order perturbation theory)-based variable-reaction-coordinate transition state theory.²⁰

The ab initio, transition-state theory-based, master-equation approach, whose application to combustion problems was pioneered by Harding and Wagner,^{21–27} is used here to obtain kinetic predictions for the thermal decomposition of the propargyl radical. This work builds on the well-developed model for the C₃H₃ reactive potential energy surface from earlier theoretical studies.^{10,12–16} However, as Harding has demonstrated,^{28,29} it is often important to use multireference electronic structure methods for treating some of the transition states. Here we employ the CASPT2 approach to explore some of the key transition states, such as that leading to ³CHCCH + H. We also pay particular attention to variational and anharmonicity effects for a number of the H loss channels and obtain higher-level energy estimates for all of the stationary points. The early master equation studies of Wagner and co-workers on the dissociation of C₂H₆²⁶ and the reaction of C₂H₅ with O₂²⁷ were instrumental to our own master-equation developments,³⁰ which are employed in the present analysis.

2. THEORY

Potential Energy Surface. Prior theoretical work on the C₃H₃ system has illuminated the key pathways for decomposition of the propargyl radical.^{10,12–16} The present electronic structure effort aims to improve the accuracy of the energetics for these pathways and to include variational treatments for the key pathways. First, the rovibrational properties of the stationary points on this C₃H₃ potential energy surface were obtained with the CCSD(T) method employing the correlation-consistent, polarized-valence, triple- ζ (cc-pVTZ) basis set of Dunning.³¹ Higher-level (HL) energy estimates for these stationary points were obtained via the consideration of a series of additive corrections. The complete-basis-set (CBS) limit was estimated from two-point extrapolation [$1/(l+1)^4$ formula³²] of CCSD(T) calculations employing aug'-cc-pVQZ and aug'-cc-pVSZ basis sets (where the prime indicates that diffuse functions are included for only the *s* and *p* orbitals in C and N and the *s* function in H) and CCSD(T)-F12³³ calculations employing the cc-pVTZ-F12 and cc-pVQZ-F12 bases.³⁴ The average of these two CBS limits, which differed by at most 0.18 kcal/mol, was used in the final analyses. A correction for higher-order excitations was obtained from CCSDT(Q)/cc-pVDZ calculations.³⁵ A correction for core–valence interactions was obtained from CCSD(T,full)/CBS calculations based on extrapolation of results for the cc-pcVTZ and cc-pcVQZ basis sets.³⁶ Anharmonic vibrational zero-point energy (ZPE) corrections were calculated at the B3LYP/cc-pVTZ level via second-order spectroscopic perturbation theory.³⁷ A relativistic correction was obtained from the difference in the singles and doubles configuration interaction (CI) energy with and without the Douglas-Kroll one-electron integrals for CI/aug-cc-pcVTZ calculations.³⁸ Diagonal Born–Oppenheimer corrections (DBOC)³⁹ were obtained at the HF/cc-pVTZ level. Detailed comparisons with values for stable species from the active thermochemical tables suggest that these HL energy estimates should have 2 σ uncertainties of ~0.3 kcal/mol.

Various difficulties were encountered in the evaluation of the correction terms for a few cases. In particular, the anharmonic ZPE calculations for CHCC, ³CHCCH, TS15, TS2P1, TS4P4, and CH did not produce meaningful values. For all but one of these cases we instead employed a correction of $-0.127 n_{\text{H}}$ kcal/mol, where n_{H} is the number of H atoms in the molecule, which was found through separate calculations for a large set of species to reproduce the structural dependence of this correction. For CH, we instead employed an MP2/cc-pVTZ value. For a few other cases, SCF convergence problems were encountered in the evaluation of the DBOC correction (TS23, TS34, TS4P4, TSSP4), or the calculated correction was unreasonably large (for *c*-CHCHCH, it was 0.44 kcal/mol). In those cases, the DBOC correction was simply ignored.

The evaluation of the role of CHCHCH presented additional difficulties. The ground state of CHCHCH is a high-spin quartet state. It is described well with single reference methods, and an HL estimate for it was readily obtained. The lowest doublet state is an open-shell state that is not described well with single reference-based methods. The energy of the doublet state was evaluated from CASPT2 evaluations of the doublet–quartet splitting and the HL energy for the quartet state. The active space for the CASPT2 evaluations consisted of the five electrons in five orbitals describing the unhybridized *p*-orbital space of the carbons. The CASPT2 estimates were extrapolated

to the CBS limit from calculations with the cc-pVQZ and cc-pVSZ bases. CASPT2 estimates for the vibrational ZPE were also employed in the HL evaluations for the quartet state due to CCSD(T) convergence problems for asymmetric geometries. Similar issues arise for the saddle point that connects c-CHCHCH with ²CHCHCH (TS26), where the calculated T1 diagnostic of 0.10 again indicates strong multireference character. This stationary point was treated in a manner similar to that used for ²CHCHCH, with a CASPT2(5e,5o)/CBS(QZ,5Z)//CASPT2(5e,5o)/cc-pVTZ evaluation of the energy of TS26 relative to ⁴CHCHCH added to the HL energy for ⁴CHCHCH.

The simple CH bond fissions in CH₂CCH produce either ³CHCCH + H or CH₂CC + H, do not have reverse barriers, and are not well-treated with single-reference methods. The CASPT2 method was used to explore the potential energy surface for these channels, employing a (7e,7o) active space whose orbitals correlate with the H radical orbital together with the *p* orbitals of the carbons (i.e, the full π -space of ³CHCCH and the π -space of CH₂CC together with the two extra carbene orbitals). The minimum energy paths (MEP) for these reactions were explored with CH-distance-constrained optimizations performed at the CASPT2(7e,7o)/cc-pVTZ level (cf. Figure 1). CBS corrections were obtained from extrapolation of

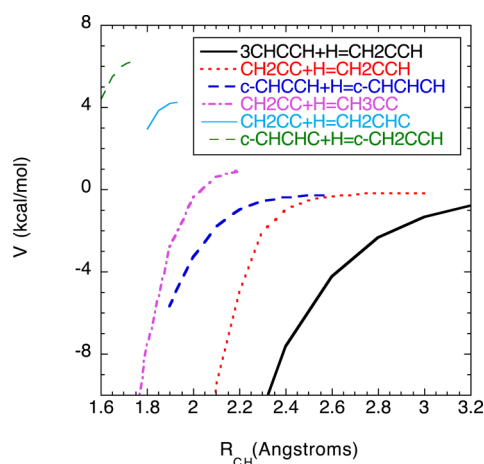


Figure 1. Plot of the minimum energy path potentials for the various CH fission channels of relevance to the decomposition of propargyl. Each of the curves are referenced to the zero-point energy of the relevant saddle point relative to its dissociation threshold, thereby emphasizing the relative ease of the reverse recombination reaction.

calculations with the cc-pVQZ and cc-pVSZ basis sets along an approximate MEP. Alternative estimates for the energy along the approximate MEP were also obtained from multireference CI calculations, from CASPT2 calculations, including an IPEA (ionization potential-electron affinity) shift⁴⁰ of 0.25 and from CCSD(T) calculations of the quartet state coupled with multireference CASPT2 and/or MRCI calculations of the doublet-quartet splittings. The MRCI results include the fixed Davidson correction for higher-order excitations. For the ³CHCCH + H channel, a geometry relaxation energy was evaluated from constrained optimizations where only the CH bending angle was optimized, with all other coordinates held fixed at their infinite separation values.

The other H loss channels each have a distinct saddle point, but this barrier relative to separated fragments is generally quite small. In this instance, it is still important to employ variational

treatments of the transition state.⁴¹ For these channels, the minimum energy path was mapped out with constrained optimizations and rovibrational analyses performed at the CCSD(T)/cc-pVTZ level with the CH separation chosen as a distinguished reaction coordinate. These minimum energy paths are also illustrated in Figure 1. For the c-CHCCH + H MEP, the CCSD(T)/CBS(QZ,5Z) limit was also determined.

The present CCSD(T) calculations generally employed RHF wave functions within the UCCSD(T) formalism implemented in MOLPRO,⁴² while the CCSDT(Q) calculations employed UHF wave functions as required by the MOLPRO implementation of Kállay's MRCC code.⁴³ The CASPT2 calculations were also performed with MOLPRO.⁴² The DBOC were obtained with the CFOUR code of Stanton and Gauss.⁴⁴ The density-functional-theory calculations were performed with G09.⁴⁵

Microcanonical Rate Coefficients. Rigid-rotor, harmonic-oscillator (RRHO) assumptions were generally employed in the evaluation of the requisite densities of states and partition functions for the molecular complexes and the number of available states for the transition state. The various CH fission channels were treated with variational transition state theory,⁴⁶ employing CH separations as a distinguished reaction coordinate.

For the ³CHCCH + H and c-CHCCH + H channels, the transition state lies at separations where RRHO assumptions are of questionable validity. Furthermore, these two channels dominate the high-temperature kinetics. Thus, these channels were treated with variable-reaction-coordinate transition-state theory (VRC-TST), which provides an accurate treatment of the full anharmonicity and rovibrational couplings for the key transitional modes. For the ³CHCCH + H channel, we employ directly determined CASPT2(7e,7o)/cc-pVTZ energies,^{47–50} while for the c-CHCCH + H channel, we employ directly determined CCSD(T)/cc-pVTZ energies. In both cases, one-dimensional corrections for basis set limitations and geometry relaxation effects were included and the final results were multiplied by a dynamical recrossing factor of 0.9.⁵¹

For both reactions, two pivot points were employed for the C₃H₂ fragments. For the ³CHCCH fragment, these pivot points were displaced along the CC axis, while for the c-CHCCH fragment, they were displaced along vectors pointing away from the lone C atom at a 45° angle with respect to the C_{2v} symmetry axis. For both reactions, a center-of-mass pivot point was employed at larger separations.

For the ³CHCCH + H reaction, the present dynamically corrected VRC-TST calculations are closely analogous to those reported in ref 20. For the c-CHCCH + H reaction, the VRC-TST results are essentially identical to corresponding RRHO-based VTST evaluations near room temperature but then gradually diverge with increasing temperature, with the VRC-TST predictions being a factor of 1.7 higher at 2000 K. The VRC-TST approach includes a full treatment of anharmonicities for the coupled bending and reaction coordinate motions and so is expected to be more accurate.

The barrierless nature of the CH₂CC + H channel suggests that it would also be appropriate to apply VRC-TST to this channel. However, as illustrated in Figure 1, the MEP for this channel is much less attractive than that for the ³CHCCH + H channel. As a result, the effective transitional-mode frequencies at the transition state are much larger for this channel, and RRHO assumptions should be more appropriate. Furthermore, the higher endothermicity and reduced attractiveness for the

MEP also indicates that this channel is of reduced kinetic importance. Thus, standard RRHO-based VTST methods incorporating the CASPT2 calculated MEP energies are employed for this channel.

Thermal Rate Coefficients. Temperature- and pressure-dependent phenomenological rate coefficients for the decomposition of C_3H_3 are obtained from the one-dimensional master equation, employing the PAPER software package.^{52,53} This package provides an automated treatment of the well-merging phenomenon and automated generation of PLOG fits (a standard format for CHEMKIN input which employs logarithmic interpolations in the pressure of temperature-dependent values obtained from modified Arrhenius representations for a grid of pressures) for incorporation into global modeling studies. The requisite Lennard–Jones collision rate parameters for CH_2CCH in two bath gases were calculated using the “one-dimensional optimization” method⁵⁴ and $C_xH_y + M$ analytic potential energy surfaces developed and validated elsewhere.⁵⁵ The calculated parameters (ϵ/cm^{-1} , $\sigma/\text{\AA}$) for $CH_2CCH + M$, $M = Ar$ and N_2 are (83.5, 4.01) and (38.3, 4.43), respectively.

Collisional energy transfer in the master equation was described using the “exponential-down” model,⁵⁶ where, within this one-dimensional (in E) model, the range parameter α for the deactivating wing of the energy transfer probability function P is approximately equal to the average energy in deactivating collisions, $\langle\Delta E_d\rangle$. A more complete description of collisional energy transfer requires more detailed, two-dimensional (in E and J) models^{57,58} for P that include: an explicit dependence on J , the nonseparability of E and J , “long tail” or biexponential dependence on E , etc. The effect of using such a model is estimated below, but a detailed application of the two-dimensional master equation is beyond the scope of the present work.

We consider three different procedures for determining α and, in each case, we represent the temperature-dependence with the expression

$$\alpha(T) = \alpha_{300}(T/300\text{ K})^n$$

The simplest procedure, which is also the most commonly employed, involves empirically estimating the parameters (α_{300} and n), either from values determined in studies of related systems or via fits of the predicted rates to experimental data. In our prior studies of C_3H_8 ,⁵⁹ C_2H_5OH ,⁶⁰ CH_3CHO ,⁶¹ CH_3OCH_3 ,⁶² and C_2H_6 ⁶³ dissociations, n was set to 0.85 and α_{300} values of 100, 125, 150, 100, and 120 cm^{-1} were found to yield reasonable representations of the experimental dissociation rates. Propargyl has a molecular size and dissociation energy similar to this set of molecules and thus might be expected to have a similar form. An α_{300} of 125 cm^{-1} is chosen as representative of these related values and will be seen to provide a reasonable representation of the limited experimental data for propargyl decomposition.

In the two other approaches, we have calculated $\langle\Delta E_d\rangle$ via full-dimensional trajectories (with initial conditions and final state analyses described in detail elsewhere^{64,65}). In the first of these, we use “universal” $C_xH_y + M$ analytic potential energy surfaces⁵⁵ and obtain $(\alpha_{300}/cm^{-1}, n) = (247, 0.85)$ and $(234, 0.88)$, for Ar and N_2 , respectively. The two-parameter expression reproduced the calculated values of $\langle\Delta E_d\rangle$ within $\sim 5\%$ from 300–3000 K. These results were obtained for an initial vibrational energy of CH_2CCH of 90 kcal/mol, which is roughly the threshold for H atom loss. Energy transfer

properties are typically weak functions of the initial energy for calculations involving vibrationally excited species. This was confirmed here, as the values of $\langle\Delta E_d\rangle$ calculated for an initial energy of 50 kcal/mol were only $\sim 10\%$ lower than those obtained for 90 kcal/mol.

The parameters for the universal interaction potential are based on $CH_4 + M$ interactions, and the resulting parametrized C–M and H–M pairwise interactions are then assumed to apply “universally” to larger hydrocarbons C_xH_y . The transferability of these parameters to larger systems was previously tested by comparing $\langle\Delta E_d\rangle$ calculated using the universal PES against direct dynamics results for C_2H_5 and C_2H_6 (with differences of $<20\%$); the universal fit was then used to study C_xH_y for x as large as 8 and $y = 2x$, $2x + 1$, and $2x + 2$.⁵⁵ In other work, the universal PES was used to predict Lennard–Jones collision rates and diffusion coefficients in good agreement with those based on tabulated and measured values for several n -alkanes.^{54,66} The accuracy of the “universal” interaction potential is less certain for highly unsaturated species like CH_2CCH .

To test its accuracy for CH_2CCH as well as the sensitivity of the present results to the parametrization of the PES, a new system-specific interaction potential was developed for $CH_2CCH + Ar$. The strategy used here was similar to the strategy used to obtain the original parametrization for $CH_4 + Ar$.⁶⁴ Briefly, cutoff Buckingham potentials were used for the two unique pairwise interactions ($Ar-C$ and $Ar-H$). The 8 parameters were optimized against 160 counterpoise-corrected QCISD(T)/CBS energies calculated along six cuts through the interaction potential. The resulting mean, unsigned, fitting error for interaction energies less than 2000 cm^{-1} was 16 cm^{-1} . This value may be compared with the mean, unsigned error of the “universal” PES of 59 cm^{-1} for the same $CH_2CCH + Ar$ data. As discussed elsewhere, the mean, unsigned, fitting error alone is not a good measure of the quality of fitted interaction potentials for energy transfer calculations, which depend more sensitively on the range of the repulsive wall.⁶⁴ A detailed comparison of the universal and newly fitted $CH_2CCH + Ar$ interaction potentials is beyond the scope of this work. Instead, we compare the results of the two fitted surfaces and use this as one measure of the uncertainty in the present approach. Using the newly fitted PES, we obtain $(\alpha_{300}/cm^{-1}, n) = (506, 0.66)$.

3. RESULTS AND DISCUSSION

3.1. Potential Energy Surface. A schematic illustration of the kinetically relevant stationary points on the potential energy surface for decomposition of propargyl is provided in Figure 2. The corresponding HL energies are reported in Table 1 together with related values from the literature. There are two primary paths for the dissociation of CH_2CCH . The lowest energy path, which is dominant at low temperatures, involves isomerization to $c-CHCHCH$ followed by dissociation to $c-CHCCH + H$. The other path, which becomes important at higher temperature, involves the direct dissociation to $^3CHCCH + H$. The product energies for these two channels are 3.4 and 1.9 kcal/mol higher, respectively, than the corresponding CCSD(T)/6-311+G(3df,2p)//B3LYP/6-311G-(d,p) energies from ref 10. The $c-CH_2CCH$, CH_2CHC , and $CHCHCH$ wells all have such low barriers to isomerization that they are unlikely to be chemically stable for all relevant temperatures. In contrast, the barriers for dissociation of $c-CHCHCH$ and CH_3CC are large enough that these species should exist to fairly high temperature.

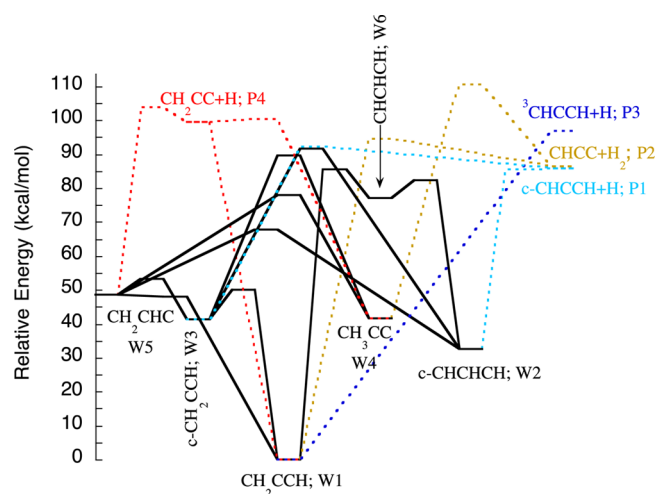


Figure 2. Schematic diagram of the potential energy surface for the decomposition of C_3H_3 . The black solid lines denote isomerization pathways, while the dashed lines denote dissociation pathways colored according to their products. In the text, the transition states are labeled by the species they connect.

In the kinetic analyses, we presume that the conversion from doublet to quartet $CHCHCH$ is relatively slow and thus ignore the latter state. Furthermore, even if the intersystem crossing is

rapid, we would not expect a major role for this state because the isomerization to $c-CHCHCH$ already occurs rapidly through the CH_2CHC isomer. Also, the CH bond fission on the quartet state to yield ${}^3CHCCH + H$ has a small positive reverse barrier making it noncompetitive with the corresponding dissociation to ${}^3CHCCH + H$ directly from propargyl, where the reverse minimum energy path is purely attractive. Nguyen et al.¹⁰ report a saddle point for the formation of ${}^3CHCCH + H$ from 2CHCHCH . Our attempts to locate this saddle point with CCSD(T) and/or CASPT2 methods instead encountered a second-order saddle point that appears either to degenerate into TS16 or into a second-order saddle point for a long-range roaming motion connecting with $c-CH_2CCH$. Regardless, this second-order saddle point lies high enough in energy to be kinetically irrelevant. Another difference from ref 10 is in the determination of a saddle point for the addition of H to CH_2CC to form CH_3CC that is slightly above the $H + CH_2CC$ asymptote. These differences appear to arise from the change from B3LYP to CCSD(T) optimizations.

On average, the stationary point energies in Table 1 are 1.4 kcal/mol higher than those from ref 10, and the RMS deviation between the two is 1.7 kcal/mol. In general, differences of this magnitude have a significant impact on kinetic predictions (e.g., at 1500 K, the Boltzmann factor is 0.5 for a 2 kcal/mol energy). It is instructive to consider the magnitude of the various

Table 1. Stationary Point Energies for the C_3H_3 Potential Energy Surface.^a

species	label	HL ^b	CCSD(T)/6-311+G(3df,2p) ^c	CCSD(T)/CBS ^d	CASPT2/ANO ^e	T1 ^f
CH_2CCH	W1	0.0	0.0	0.0	0.0	0.025
$c-CHCHCH$	W2	32.5	31.3		34.7	0.014
$c-CH_2CCH$	W3	41.4	40.1		42.3	0.019
CH_3CC	W4	41.7	40.1	40.8	40.5	0.014
CH_2CHC	W5	48.5	46.9	47.7	47.1	0.028
4CHCHCH		72.6				0.017
2CHCHCH	W6	77.1 ^g	76.3	82.1	70.9	
$c-CHCCH + H$	P1	85.8	82.4		87.5	0.011
$CHCC + H_2$	P2	86.3	84.0	83.6	85.4	0.039 ^f
${}^3CHCCH + H$	P3	96.8	94.9		89.6	0.023
$CH_2CC + H$	P4	99.5	95.9		96.2	0.019
$CH(^2\Pi) + C_2H_2$	P5	111.9	108.6		109.0	0.009
TS13		50.1	49.6		48.3	0.035
TS15		48.1	46.6	44.3	46.9	0.028
TS16		85.6	86.8	86.2	84.4	0.039 ^f
TS1P2		94.6	94.2	94.2	93.1	0.032
TS23		91.7	90.6			0.020
TS25		67.8	66.4		67.7	0.026
TS26		82.3 ^g	83.3		74.8	0.097 ^h
TS2P1		85.5 ⁱ	82.5		91.0	0.013
TS34		89.7	88.3		91.1	0.041 ^f
TS35		53.3	51.8		53.4	0.021
TS3P1		92.1 ⁱ	93.1		93.4	0.019
TS45		78.1	76.5	76.7	77.9	0.015
TS4P2		110.4	110.4	110.4	109.3	0.041 ^f
TS4P4		100.4 ⁱ	–		96.4	0.021
TS5P4		103.7 ⁱ	101.1			0.023

^aEnergies are in kcal/mol and include zero-point corrections. ^bHL energies are calculated as described in the text. ^cCCSD(T)/6-311+G(3df,2p)//B3LYP/6-311G(d,p) are from ref 10. ^dCCSD(T)/CBS(T,Q)//BH&HLYP/cc-pVQZ are from ref 12. ^eCASPT2(11e,11o)/ANO//B3LYP/6-31G(d,p) calculations are from ref 14. ^fT1 Diagnostic. Quantities with a T1 diagnostic greater than 0.035. ^gOn the basis of a CASPT2(Se,So)/CBS(QZ,SZ)//CASPT2(Se,So)/cc-pVTZ, calculation of the energy relative to 4CHCHCH and an HL calculation of the energy of 4CHCHCH . ^hT1 diagnostic for CCSD(T) saddlepoint, but CASPT2 calculations replace HL calculations as described in footnote g. ⁱTransition states that were also treated variationally.

Table 2. Energy Corrections in HL Evaluations for the C₃H₃ Potential Energy Surface^a

species ^b	label	core–valence ^c	CBS ^d	T(Q)/DZ ^e	anharm. ZPE ^f	relativ. ^g	DBOC ^h	total ⁱ
CH ₂ CCH	W1	0	0	0	0	0	0	0
c-CHCHCH	W2	0.23	−0.63	0.27	−0.20	0.05	0.0	−0.29
c-CH ₂ CCH	W3	0.51	−0.08	0.07	−0.16	0.02	0.02	0.37
CH ₃ CC	W4	0.26	0.55	−0.01	−0.14	0.02	−0.03	0.64
CH ₂ CHC	W5	0.84	0.82	−0.14	−0.15	−0.08	0.01	1.29
⁴ CHCHCH		0.55	1.68	0.09	−0.14	0.00	−0.01	2.17
c-CHCCH+H	P1	0.67	−0.24	0.34	0.00	−0.06	−0.04	0.68
CHCC+H ₂	P2	0.97	1.41	−0.84	0.02	−0.14	0.00	1.42
³ CHCCH+H	P3	0.12	1.35	0.01	−0.02	−0.02	0.01	1.45
CH ₂ CC+H	P4	0.88	1.45	−0.32	0.01	−0.12	0.01	1.93
CH(² Π)+C ₂ H ₂	P5	2.02	2.08	−0.35	0.21	−0.26	0.09	3.79
Average ^j		0.71	0.84	−0.09	−0.06	−0.06	0.01	1.34
RMS ^k		0.87	1.20	0.34	0.13	0.11	0.03	1.72
TS13		0.57	−0.24	−0.45	−0.09	−0.04	0.01	−0.23
TS15		0.82	0.77	−0.12	−0.15	−0.08	0.01	1.25
TS16		0.80	0.46	−1.79	−0.37	−0.06	0.08	−0.88
TS1P2		0.88	0.36	−0.58	−0.18	−0.13	0.20	0.55
TS23		0.89	−0.37	0.11	−0.28	−0.02	0.00	0.33
TS25		0.92	0.00	−0.15	−0.16	−0.06	0.00	0.55
TS2P1		0.67	−0.51	0.30	−0.15	−0.05	−0.04	0.23
TS34		1.03	0.12	−0.25	−0.21	−0.06	0.00	0.63
TS35		0.89	0.22	−0.11	−0.14	−0.07	0.02	0.81
TS3P1		0.77	−0.78	0.16	−0.11	−0.05	0.01	0.00
TS45		0.83	0.16	−0.18	−0.06	−0.08	0.12	0.63
TS4P2		1.02	0.16	−1.23	−0.28	−0.12	0.09	−0.35
TS4P4		0.91	0.93	−0.49	−0.15	−0.12	0.00	1.09
TSSP4		1.00	0.83	−0.51	−0.15	−0.12	0.00	1.06
average ^l		0.86	0.15	−0.38	−0.18	−0.08	0.04	0.41
RMS ^m		0.87	0.51	0.66	0.19	0.08	0.07	0.71
average ⁿ		0.79	0.44	−0.26	−0.13	−0.07	0.02	0.80
RMS ^o		0.87	0.87	0.55	0.17	0.09	0.06	1.24

^aEnergies are relative to the ground state of propargyl and are in kcal/mol. ^bTransition states are labeled according to the species that they connect. ^cThe correction for core–valence correlation evaluated for the CBS limit. ^dThe difference between the CCSD(T)/CBS and CCSD(T)/cc-pVTZ energies. ^eThe UCCSDT(Q)/cc-pVDZ energy correction calculated relative to the RUCSDT(Q)/cc-pVDZ energy. ^fThe B3LYP/6-311++G(d,p)-based spectroscopic perturbation theory-based anharmonic zero-point energy correction. ^gThe CISD calculated relativistic correction. ^hThe HF/cc-pVTZ calculated diagonal Born–Oppenheimer correction. ⁱThe sum of the corrections in the other columns. ^jThe average correction for the minima. ^kThe root-mean-square correction for the minima. ^lThe average correction for the saddle points. ^mThe root-mean-square correction for the saddle points. ⁿThe average correction for all the stationary points. ^oThe root-mean-square correction for all the stationary points.

correction terms that make up the present HL energy scheme (cf. Table 2). These corrections decrease in importance across the series: core–valence > CBS > CCSDT(Q)/cc-pVDZ > vibrational anharmonicity > relativistic > DBOC, with RMS corrections of 0.87, 0.87, 0.55, 0.17, 0.09, and 0.06, respectively. The RMS magnitude of the total correction is 1.24 kcal/mol, which is clearly large enough to affect kinetic predictions. For combustion kinetics purposes, it appears important to evaluate the core–valence, CBS and CCSDT(Q) corrections. Not surprisingly, the CCSDT(Q) correction for the saddle points is larger than the corresponding correction for the minima, which may correlate with an increased uncertainty in the energy predictions, because this correction for higher-order excitations may not be converged with respect to either the basis set or the level of excitation. Interestingly, the CBS correction for the saddle points is actually substantially smaller than that for the minima, while the core–valence corrections are about the same. It is difficult to ascertain the uncertainty for the saddle points, but presuming an uncertainty of about twice that for the minima (i.e., a 2σ uncertainty of about 0.5 kcal/mol) seems reasonable.

3.2. High Pressure Kinetics. The predicted high-pressure-limit recombination rate constants are plotted in Figure 3 for the reverse of the various CH bond fission reactions of relevance to propargyl dissociation. The predicted rate constants are seen to be ordered according to their minimum energy path potentials, which were plotted in Figure 1, with the more strongly attractive potentials having the larger rate coefficients. The rate coefficient for the ³CHCCH + H channel is a factor of 2 to 3 greater than that for the c-CHCCH + H → c-CHCHCH channel. As a result, the primary products in the thermal decomposition kinetics gradually transform from c-CHCCH + H to ³CHCCH + H as the temperature is increased. The formation of CH₂CC + H from propargyl may also play some role at higher temperatures.

For the CH₂CCH → ³CHCCH + H channel, we have explored the effect of various alternative methods [CASPT2 with and without an IPEA shift, Davidson corrected MRCI, CCSD(T) calculations of the quartet state coupled with either CASPT2 or Davidson corrected MRCI calculations of the splitting] for determining the potential energy surface. The deviation in the MEP potential values from one calculation to

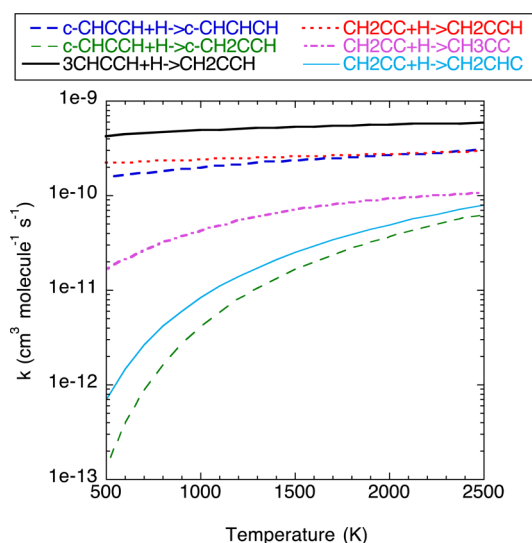


Figure 3. Plot of the calculated high pressure addition rate constants for the various H atom recombination reactions of relevance to the thermal decomposition of propargyl radical.

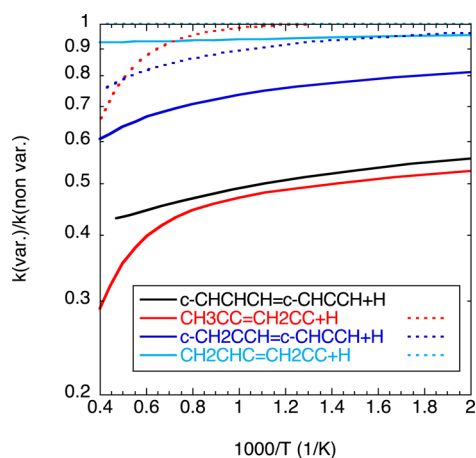


Figure 4. Plot of the calculated variational effect for the high pressure addition reactions with a saddle point. The solid lines use the saddle point on the PES, which is the standard location determined with electronic structure codes, for a reference. The dashed lines use the saddle point on the relevant ZPE-corrected PES for a reference, which leads to a lower reference rate constant and thus a variational effect that is closer to unity and that approaches it as the temperature decreases toward 0.

the next was 10% or less in the transition-state region. Notably, we have repeatedly found in similar calculations for other barrierless reactions that the percent variation in the predicted rate constants roughly matches this variation in the predicted MEP values. This effect arises from a balance between Boltzmann factors, entropies, and varying transition state location. Similar considerations for the $\text{CH}_2\text{CCH} \rightarrow \text{CH}_2\text{CC} + \text{H}$ indicate a much larger variation of up to about 30%. However, this channel is of relatively minor importance to the kinetics.

As was first pointed out by Vereecken et al.,^{14,15} it is important to include variational treatments of the transition states for all the CH bond fission reactions, including those that have saddle points. The temperature dependence of the variational effect (defined here as the ratio of the variationally optimized rate constant to that for some fixed-reference

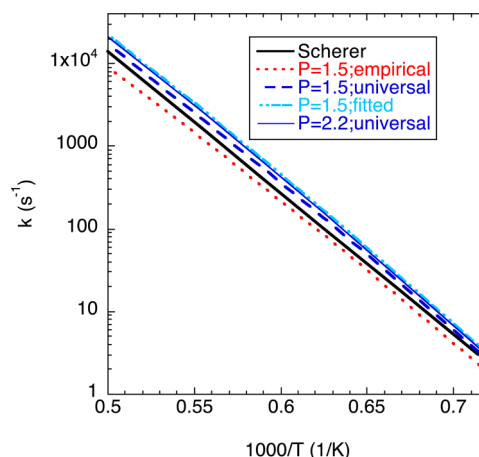


Figure 5. Temperature dependence of the rate constant for formation of H in the thermal decomposition of CH_2CCH . The calculations are for a variety of assumptions regarding the energy transfer parameters as discussed in the text. For the parameters based on the universal PES results are presented for pressures of 1.5 or 2.2 atm, which corresponds to the pressure range in the experimental study of Scherer et al.⁸ The remaining calculations are all for a pressure of 1.5 atm.

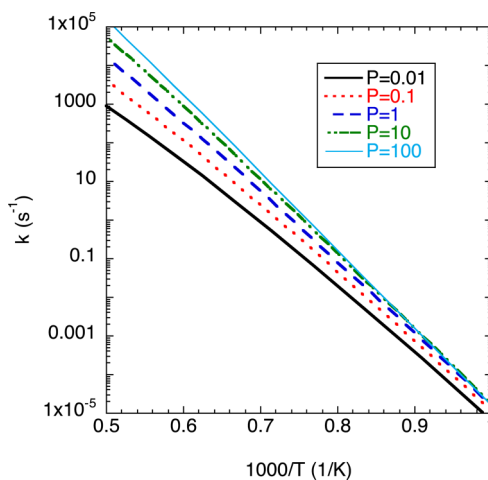


Figure 6. Temperature dependence of the total rate constant for bimolecular product formation in the decomposition of propargyl at a variety of pressures.

transition state) for the latter channels is illustrated in Figure 4. This variational effect may be defined relative to either the saddle point in the electronic PES or in the zero-point corrected PES. The latter leads to a variational effect that by definition approaches unity as the temperature decreases to 0. However, the former is more informative as it illustrates the error that one makes when employing the electronic saddle point that is generally obtained from electronic structure codes. The deviation of the variational effect from unity tends to be more significant the lower the barrier is for the reverse recombination reaction. For example, the $\text{c-CHCCH} + \text{H} \rightarrow \text{c-CHCCH}$ reaction barely has a saddle point, and in this case, the variational treatments yields a reduction in the rate constant by more than a factor of 2 for temperatures of 1000 K or higher.

3.3. Pressure-Dependent Kinetics. Scherer et al.⁸ have probed the production of H atoms arising from propargyl decomposition in Ar bath gas for temperatures ranging from

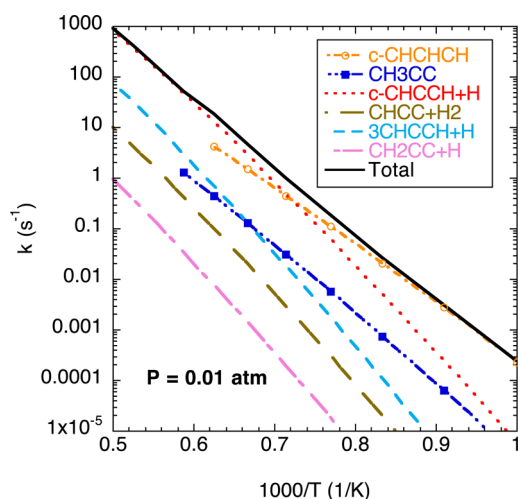


Figure 7. Temperature dependence of the elementary rate constants for decomposition of propargyl at a pressure of 0.01 atm.

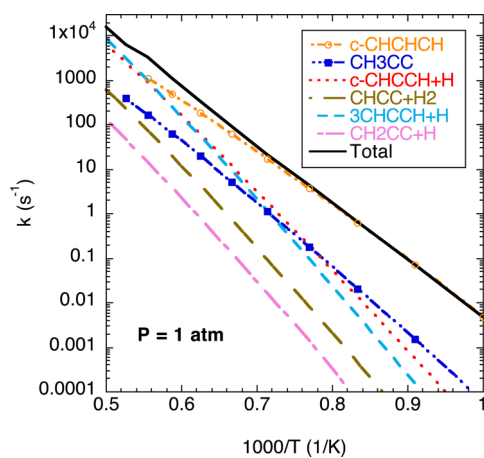


Figure 8. Temperature dependence of the elementary rate constants for decomposition of propargyl at a pressure of 1 atm.

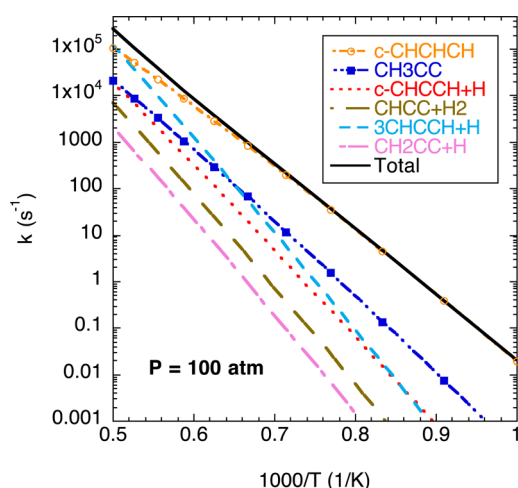


Figure 9. Temperature dependence of the elementary rate constants for decomposition of propargyl at a pressure of 100 atm.

1400 to 2000 K and pressures of 1.5 to 2.2 atm in a shock tube study of 3-iodo-propyne pyrolysis. The present predictions for the rate of dissociation to H atoms are compared with these shock tube measurements in Figure 5. These calculations

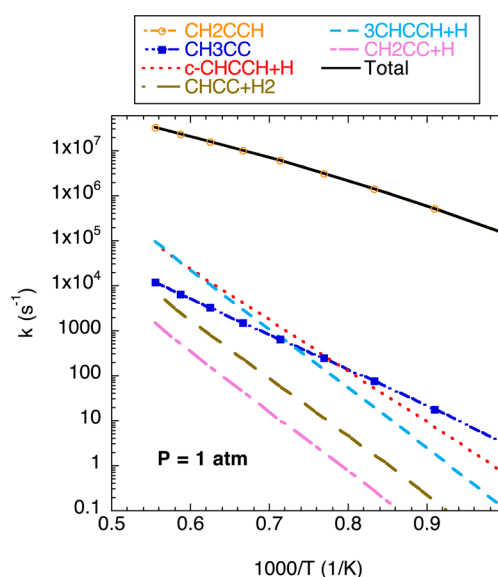


Figure 10. Temperature dependence of the elementary rate constants for decomposition of c-CHCHCH at a pressure of 1 atm.

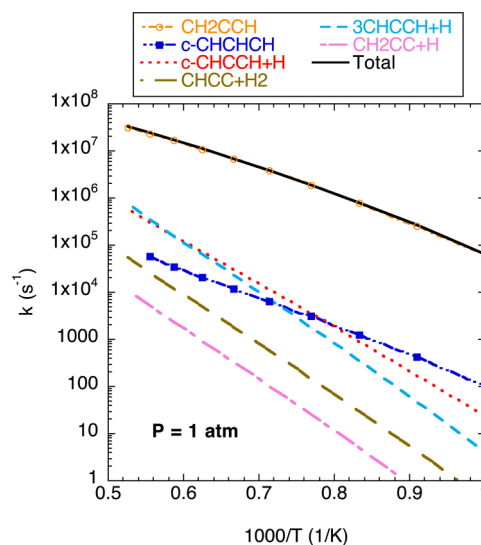


Figure 11. Temperature dependence of the elementary rate constants for decomposition of CH_3CC at a pressure of 1 atm.

consider the sum of the phenomenological rate coefficients for producing the various different H atom channels from propargyl. Some H atoms might also be produced through a sequential isomerization to c-CHCHCH followed by its dissociation. However, estimates for the contribution from this channel based on a presumed rapid pre-equilibration of c-CHCHCH and CH_2CCH yield a negligible contribution to the total rate for H production for the temperatures and pressures of relevance to this comparison with experiment.

The predictions for the empirical energy transfer model (with $\alpha = 491 \text{ cm}^{-1}$ at 1500 K) are seen to be about 1.1 to 1.5 times too small for a pressure P of 1.5 atm. In contrast, the predictions based on the energy transfer parameters arising from the universal PES (with $\alpha = 970 \text{ cm}^{-1}$ at 1500 K) are instead about 1.1 to 1.3 times too high for the same pressure. The corresponding results for 2.2 atm are up to 30% higher. Meanwhile, the results at $P = 1.5 \text{ atm}$ for the newly fitted PES (with $\alpha = 1464 \text{ cm}^{-1}$ at 1500 K), which has the most accurate

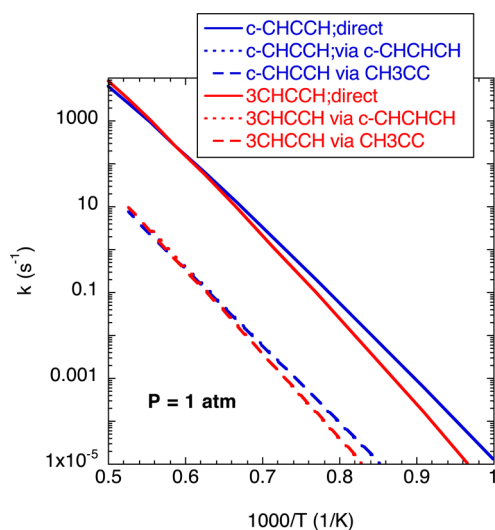


Figure 12. Plot of effective rate constants for sequential and direct bimolecular product formation from propargyl at a pressure of 1 atm.

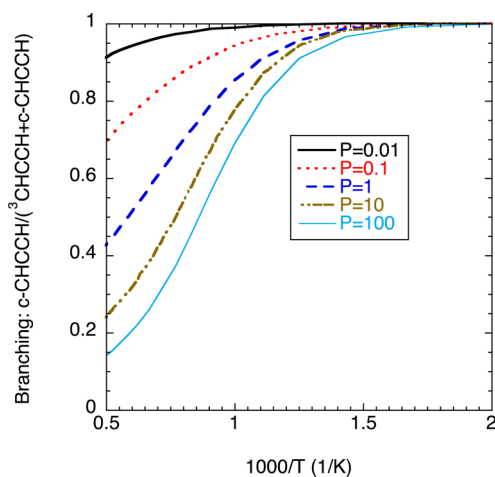


Figure 13. Temperature and pressure dependence of the branching ratio between formation of $c\text{-CHCCH} + \text{H}$ or ${}^3\text{CHCCH} + \text{H}$ in the thermal decomposition of propargyl.

description of the $\text{CH}_2\text{CCH} + \text{Ar}$ interaction, are essentially identical to those for $P = 2.2$ atm with the universal PES.

The somewhat larger discrepancy for the newly fitted PES case likely suggests that our neglect of various other factors in the calculations is important. In particular, the proper consideration of angular-momentum constraints is expected to yield a reduction in the predicted rate constant. The application of the $2\text{D}/\rho$ model [a 2-dimensional master eq (2DME) with a microcanonical strong collider in J assumption]⁶⁷ to a model one well, one-channel dissociation to ${}^3\text{CHCCH} + \text{H}$ yields only a minor reduction of 5% to 10% from the corresponding 1-dimensional master equation model for the temperature and pressure range of relevance to the experiment of Scherer et al.⁸ However, a complete two-dimensional treatment, accounting for nonseparability of E and J transfer probabilities and deviation from the strong-collider-in- J assumption, will yield even smaller rate coefficients.⁵⁸ For the present case, the effect of such a full 2DME treatment on the low pressure limit⁶⁵ was calculated for the model one well, one-channel system describing the dissociation of CH_2CCH to ${}^3\text{CHCCH} + \text{H}$. These calculations suggest that the $2\text{D}/\rho$

model predictions are too high by a factor of 2.8–1.6 at 1000–2000 K. However, this reduction is counterbalanced by the present neglect of the effect of vibrational anharmonicities on the density of states for the complex in the master equation calculations. This effect was approximated as the anharmonic correction to ρ/Q , where ρ is the state density of CH_2CCH at 90 kcal/mol (near its dissociation threshold) and Q is the partition function for CH_2CCH . This anharmonic correction was calculated using Monte Carlo phase space integration in curvilinear coordinates⁶⁸ and was found to vary from 1.9–1.4 for 1000–2000 K. The overall correction from both effects varies from 0.66–0.87 for 1000–2000 K. This correction is likely similar to or smaller than other sources of uncertainty in the trajectory-based calculation of the energy transfer parameters, which may contribute up to a 50% uncertainty in the low-pressure limit rate predictions.

On the basis of these considerations, we suggest that the 2σ overall uncertainty in our predicted low-pressure limit is about a factor of 2. Of course, the error in the thermal rate prediction associated with the treatment of collisional energy transfer decreases at higher pressures. Nevertheless, the 2σ uncertainty in the predicted high pressure limit for the $\text{CH}_2\text{CCH} \rightarrow {}^3\text{CHCCH} + \text{H}$ rate coefficient is still about a factor of 2 due to the uncertainty of perhaps 30% in the transition state partition function, the neglect of the anharmonic contribution to the propargyl canonical partition function, and the uncertainty in the dissociation energy. Thus, it seems prudent to simply assign a 2σ uncertainty of a factor of 2 for the full temperature and pressure range of the current predictions. Clearly, the observed discrepancy between the fitted PES-based predictions and the experimental results is still well within the uncertainties of the theoretical predictions, especially when one accounts for the fact that there are likely significant uncertainties in the experimental results as well.

For our final predictions of the decomposition rates in the N_2 bath gas, we have chosen to use the energy transfer parameters for the universal potential, since these results give the best agreement with the results of Scherer et al.⁸ Furthermore, these predictions fall somewhere between those from the empirical energy transfer model and from the fitted PES energy transfer model. The temperature and pressure dependence of the calculated total propargyl decomposition rate is illustrated in Figure 6. At 1000 K, the reaction is nearly pressure-independent for pressures of 0.1 atm or higher, while at 2000 K, the reaction is well into falloff even for a pressure of 100 atm.

The temperature-dependence of the individual component rate constants is illustrated in Figures 7, 8, and 9 for pressures of 0.01, 1, and 100 atm, respectively. Note that the $c\text{-CH}_2\text{CCH}$, CH_2CHC , and CHCHCH species all become chemically unstable at fairly low temperature [i.e., by 700 K even at 100 atm (note that by chemically unstable we mean that they cannot persist as a unique species over a collisional timescale because the corresponding chemically significant eigenvalue lies in the quasi-continuum of internal energy relaxation rates)]. Thus, we do not report rate constants for production of any of these species. In contrast, the $c\text{-CHCHCH}$ ring and CH_3CC are stable to much higher temperature; for pressures of 1 atm and higher, they are stable to at least 1800 K. The unimolecular isomerization to the cyclic ring $c\text{-CHCHCH}$ dominates the kinetics, at least for temperatures below its stability limit. At higher temperatures, production of $c\text{-CHCCH} + \text{H}$ and of ${}^3\text{CHCCH} + \text{H}$ become important, with the latter being more important at high pressure. The $\text{CH}_2\text{CC} + \text{H}$ and $\text{CHCC} + \text{H}_2$

Table 3. Modified Arrhenius Parameters for CH₂CCH Dissociation Rate Coefficients^a

reaction	pressure (atm)	A (s ⁻¹)	n	E _a (cal/mol)	T-range (K)
CH ₂ CCH → c-CHCCH + H	0.001	4.40 × 10 ⁴²	-9.05	96280	600–2000
	0.003	3.82 × 10 ⁴¹	-8.61	96480	600–2000
	0.01	9.71 × 10 ³⁹	-8.03	96460	600–2000
	0.03	1.33 × 10 ³⁸	-7.39	96150	600–2000
	0.1	4.77 × 10 ³⁵	-6.59	95490	600–2000
	0.3	1.37 × 10 ³³	-5.79	94600	600–2000
	1	1.33 × 10 ³⁰	-4.87	93410	600–2000
	3	2.07 × 10 ²⁷	-4.01	92210	600–2000
	10	2.49 × 10 ²⁴	-3.13	90950	600–2000
	30	2.15 × 10 ²²	-2.49	90290	600–2000
CH ₂ CCH → ³ CHCCH + H	0.001	2.10 × 10 ³⁷	-7.68	105400	600–2000
	0.003	3.94 × 10 ³⁹	-8.14	105700	600–2000
	0.01	5.43 × 10 ⁴¹	-8.53	106600	600–2000
	0.03	6.97 × 10 ⁴²	-8.65	107600	600–2000
	0.1	1.19 × 10 ⁴³	-8.52	108400	600–2000
	0.3	2.69 × 10 ⁴²	-8.18	108900	600–2000
	1	6.46 × 10 ⁴⁰	-7.55	108900	600–2000
	3	3.49 × 10 ³⁸	-6.78	108500	600–2000
	10	1.70 × 10 ³⁵	-5.71	107600	600–2000
	30	4.43 × 10 ³¹	-4.59	106200	600–2000
100	3.38 × 10 ²⁷	-3.33	104500	600–2000	

^aRate coefficient is given by $AT^n \exp(-E_a/RT)$, where T is in K.

channels never contribute more than a few percent to the total rate, while the CH₃CC channel contributes at most 10%.

Phenomenologically, the formation of the bimolecular products may occur either directly (e.g., CH₂CCH → CHCCH + H) or sequentially (e.g., through the sequence CH₂CCH → c-CHCHCH → CHCCH + H). To explore the role of the sequential formation, we plot in Figures 10 and 11 the rate constants for decomposition of c-CHCHCH and CH₃CC, respectively. For both of these species, the isomerization back to CH₂CCH dominates the kinetics, suggesting that the sequential process will involve a pre-equilibrium between CH₂CCH and the relevant intermediate. In this instance, one may estimate the overall rate for the sequential process as the product of the equilibrium constant with the dissociation rate constant. This product is plotted in Figure 12 together with the corresponding phenomenological direct rate constant. Clearly the formation of c-CHCCH + H and of ³CHCCH + H effectively occur through only the well-skipping direct mechanism. At very low temperatures and high pressure, the sequential pathways do eventually become relevant (e.g., 500 K and 100 atm), but for combustion relevant conditions, they are insignificant.

The temperature and pressure dependence of the branching between the two primary bimolecular product channels is illustrated in Figure 13. At low temperature or low pressure, the formation of c-CHCCH + H dominates because of the lower thresholds for this channel. At higher temperature and high pressure, the ³CHCCH + H channel dominates because its direct formation from CH₂CCH avoids any tight transition states such as that required to form the 3-membered ring species.

For kinetic modeling purposes, we report in Table 3, modified Arrhenius representations of the rate constants for CH₂CCH → c-CHCCH + H and CH₂CCH → ³CHCCH + H for a wide range of pressures. These expressions should allow for the implementation of the present predictions into global

modeling codes such as CHEMKIN through their PLOG format.

CONCLUSION

Using high-level electronic-structure methods, variational transition-state theory, classical trajectories for energy transfer, and multiple-well master-equation methodology, we have determined phenomenological (thermal) rate coefficients for the dissociation of propargyl (CH₂CCH) over a wide range of conditions. The methods are described at some length in the paper. Propargyl dissociates primarily into two different sets of products: ³CHCCH + H and c-CHCCH + H. The latter is a well-skipping reaction and dominates under low-pressure and/or low-temperature conditions; the former is a direct channel and dominates under high-temperature and/or high-pressure conditions. The contribution to formation of the latter products by a sequential isomerization (stabilization)/dissociation process is negligible. The rate constants are given in PLOG format for use in chemical kinetic modeling.

ASSOCIATED CONTENT

Supporting Information

PAPER input file for the C₃H₃ PES considered here; number of states for the c-CHCCH + H channel; and number of states for the ³CHCCH + H channel. This material is available free of charge via the Internet at <http://pubs.acs.org>.

AUTHOR INFORMATION

Corresponding Author

*E-mail: jim.miller1946@gmail.com.

Notes

The authors declare no competing financial interest.

ACKNOWLEDGMENTS

This material is based upon work supported by the U.S. Department of Energy, Office of Science, Office of Basic Energy Sciences, Division of Chemical Sciences, Geosciences, and Biosciences under Contract DE-AC02-06CH11357. Sandia is a multiprogram laboratory operated by Sandia Corporation, a Lockheed Martin Company, for the United States Department of Energy under Contract DE-AC04-94-AL85000.

REFERENCES

- (1) Hansen, N.; Miller, J. A.; Klippenstein, S. J.; Westmoreland, P. R.; Kohse-Hoinghaus, K. Exploring Formation Pathways of Aromatic Compounds in Laboratory-Based Model Flames of Aliphatic Fuels. *Combustion, Explosion, and Shock Waves* **2012**, *48*, 508–515.
- (2) Zhang, H. R.; Eddings, E. G.; Sarofim, A. F.; Westbrook, C. K. Fuel Dependence of Benzene Pathways. *Proc. Combust. Inst.* **2009**, *32*, 377–385.
- (3) Miller, J. A.; Pilling, M. J.; Troe, J. Unravelling Combustion Mechanisms through a Quantitative Understanding of Elementary Reactions. *Proc. Combust. Inst.* **2005**, *30*, 43–88.
- (4) Pope, C. J.; Miller, J. A. Exploring Old and New Benzene Formation Pathways in Low-Pressure Premixed Flames of Aliphatic Fuels. *Proc. Combust. Inst.* **2000**, *28*, 1519–1527.
- (5) Miller, J. A.; Melius, C. F. Kinetic and Thermodynamic Issues in the Formation of Aromatic Compounds in Flames of Aliphatic Fuels. *Combust. Flame* **1992**, *91*, 21–39.
- (6) Matsugi, A.; Miyoshi, A. Computational Study of the Recombination Reaction Between Benzyl and Propargyl Radicals. *Int. J. Chem. Kin.* **2012**, *44*, 206–218.
- (7) Note that the bond energies summarized in this paragraph come from our own high level calculations such as are summarized in the present work.
- (8) Scherer, S.; Just, Th.; Frank, P. High-Temperature Investigations of Pyrolytic Reactions of Propargyl Radicals. *Proc. Combust. Inst.* **2000**, *28*, 1511–1518.
- (9) Deyerl, H. J.; Fischer, I.; Chen, P. Photodissociation Dynamics of the Propargyl Radical. *J. Chem. Phys.* **1999**, *111*, 3441–3448.
- (10) Nguyen, T. L.; Mebel, A. M.; Lin, S. H.; Kaiser, R. I. Product Branching Ratios of the $C(^3P) + C_2H_3(^2A')$ and $CH(^2\Pi) + C_2H_2(^1\Sigma_g^+)$ Reactions and Photodissociation of $H_2CCCH(^2B_1)$ at 193 and 242 nm: An Ab Initio/RRKM Study. *J. Phys. Chem. A* **2001**, *105*, 11549–11559.
- (11) McCunn, L. R.; FitzPatrick, B. L.; Krisch, M. J.; Butler, L. J.; Liang, C.-W.; Lin, J. J. Unimolecular Dissociation of the Propargyl Radical Intermediate of the $CH + C_2H_2$ and $C + C_2H_3$ Reactions. *J. Chem. Phys.* **2006**, *125*, 133306.
- (12) Castiglioni, L.; Vukovic, S.; Crider, P. E.; Lester, W. A.; Neumark, D. M. Intramolecular Competition in the Photodissociation of C_3D_3 Radicals at 248 and 193 nm. *Phys. Chem. Chem. Phys.* **2010**, *12*, 10714–10722.
- (13) Guadagnini, R.; Schatz, G. C.; Walch, S. D. Ab Initio and RRKM Studies of the Reactions of C, CH, and 1CH_2 with Acetylene. *J. Phys. Chem. A* **1998**, *102*, 5857–5866.
- (14) Vereecken, L.; Pierloot, K.; Peeters, J. B3LYP-DFT Characterization of the Potential Energy Surface of the $CH(X^2\Pi) + C_2H_2$ Reaction. *J. Chem. Phys.* **1998**, *108*, 1068–1080.
- (15) Vereecken, L.; Peeters, J. Detailed Microvariational RRKM Master Equation Analysis of the Product Distribution of the $C_2H_2 + CH(X^2\Pi)$ Reaction over Extended Temperature and Pressure Ranges. *J. Phys. Chem. A* **1999**, *103*, 5523–5533.
- (16) Goulay, F.; Trevitt, A. J.; Meloni, G.; Selby, T. M.; Osborn, D. L.; Taatjes, C. A.; Vereecken, L.; Leone, S. R. Cyclic Versus Linear Isomers Produced by Reaction of the Methylidyne Radical (CH) with Small Unsaturated Hydrocarbons. *J. Am. Chem. Soc.* **2009**, *131*, 993–1005.
- (17) Maksyutenko, P.; Zhang, F.; Gu, X.; Kaiser, R. I. A Crossed Molecular Beam Study on the Reaction of Methylidyne Radicals [$CH(X^2\Pi)$] with Acetylene [$C_2H_2(X^1\Sigma_g^+)$]: Competing $C_3H_2 + H$ and $C_3H + H_2$ Channels. *Phys. Chem. Chem. Phys.* **2011**, *13*, 240–252.
- (18) Nguyen, T. L.; Mebel, A. M.; Kaiser, R. I. A Theoretical Investigation of the Triplet Carbon Atom $C(^3P) +$ Vinyl Radical $C_2H_3(^2A')$ Reaction and Thermochemistry of C_3H_n ($n = 1-4$) Species. *J. Phys. Chem. A* **2001**, *105*, 3284–3299.
- (19) Kiefer, J. H.; Mudipalli, P. S.; Sidhu, S. S.; Kern, R. D.; Jursic, B. S.; Xie, K.; Chen, H. Unimolecular Dissociation in Allene and Propyne: The Effect of Isomerization on the Low Pressure Rate. *J. Phys. Chem. A* **1997**, *101*, 4057–4071.
- (20) Harding, L. B.; Klippenstein, S. J.; Georgievskii, Y. On the Combination Reaction of Hydrogen Atoms with Resonance-Stabilized Hydrocarbon Radicals. *J. Phys. Chem. A* **2007**, *111*, 3789–3801.
- (21) Walch, S. P.; Wagner, A. F.; Dunning, T. H.; Schatz, G. C. Theoretical Studies of the $O + H_2$ Reaction. *J. Chem. Phys.* **1980**, *72*, 2894–2896.
- (22) Harding, L. B.; Schatz, G. C. An Ab Initio Determination of the Rate-Constant for $H + H_2CO \rightarrow H_2 + HCO$. *J. Chem. Phys.* **1982**, *76*, 4296–4297.
- (23) Harding, L. B.; Wagner, A. F.; Bowman, J. M.; Schatz, G. C.; Christoffel, K. Ab Initio Calculation of the Transition State Properties and Rate Constants for $H + C_2H_2$ and Selected Isotopic Analogs. *J. Phys. Chem.* **1982**, *86*, 4312–4327.
- (24) Harding, L. B.; Wagner, A. F. Theoretical Studies on the Reaction of Atomic Oxygen ($O(^3P)$) + C_2H_2 . 2. *J. Phys. Chem.* **1986**, *90*, 2974–2987.
- (25) Wagner, A. F.; Bowman, J. M. The Addition and Dissociation Reaction $H + CO = HCO$. 1. Theoretical RRKM Studies. *J. Phys. Chem.* **1987**, *91*, 5314–5324.
- (26) Wagner, A. F.; Wardlaw, D. M. Study of the Recombination Reaction $CH_3 + CH_3 \rightarrow C_2H_6$. 2. Theory. *J. Phys. Chem.* **1988**, *92*, 2462–2471.
- (27) Wagner, A. F.; Slagle, I. R.; Sarzynski, D.; Gutman, D. Experimental and Theoretical Studies of the $C_2H_5 + O_2$ Reaction-Kinetics. *J. Phys. Chem.* **1990**, *94*, 1853–1868.
- (28) Harding, L. B.; Klippenstein, S. J.; Jasper, A. W. Ab Initio Methods for Reactive Potential Surface. *Phys. Chem. Chem. Phys.* **2007**, *9*, 4055–4070.
- (29) Harding, L. B.; Klippenstein, S. J.; Miller, J. A. Kinetics of $CH + N_2$ Revisited with Multireference Methods. *J. Phys. Chem. A* **2008**, *112*, 522–532.
- (30) Miller, J. A.; Klippenstein, S. J. Master Equation Methods in Gas Phase Chemical Kinetics. *J. Phys. Chem. A* **2006**, *110*, 10528–10544.
- (31) Dunning, T. H. Gaussian-basis Sets for Use in Correlated Molecular Calculations. 1. The Atoms Boron through Neon and Hydrogen. *J. Chem. Phys.* **1989**, *90*, 1007–1023.
- (32) Martin, J. M. L.; Uzan, O. Basis Set Convergence in Second-Row Compounds. The Importance of Core Polarization Functions. *Chem. Phys. Lett.* **1998**, *282*, 16–24.
- (33) Knizia, G.; Adler, T. B.; Werner, H.-J. Simplified CCSD(T)-F12 Methods: Theory and Benchmarks. *J. Chem. Phys.* **2009**, *130*, 054104.
- (34) Peterson, K. A.; Adler, T. B.; Werner, H.-J. Systematically Convergent Basis Sets for Explicitly Correlated Wavefunctions: The Atoms H, He, B-Ne, and Al-Ar. *J. Chem. Phys.* **2008**, *128*, 084102.
- (35) Bomble, Y. J.; Stanton, J. F.; Kállay, M.; Gauss, J. Coupled-Cluster Methods Including Noniterative Corrections for Quadruple Excitations. *J. Chem. Phys.* **2005**, *123*, 054101.
- (36) Woon, D. E.; Dunning, T. H. Gaussian-basis Sets for Use in Correlated Molecular Calculations. 5. Core-Valence Basis-sets for Boron through Neon. *J. Chem. Phys.* **1995**, *103*, 4572–4585.
- (37) Bloino, J.; Biczysko, M.; Barone, V. General Perturbative Approach for Spectroscopy, Thermodynamics and Kinetics: Methodological Background and Benchmark Studies. *J. Chem. Theory Comput.* **2012**, *8*, 1015–1036.
- (38) Cowan, R. D.; Griffin, D. C. Approximate Relativistic Corrections to Atomic Radial Wave-Functions. *J. Opt. Soc. Am.* **1976**, *66*, 1010–1014.
- (39) Handy, N. C.; Yamaguchi, Y.; Schaefer, H. F. The Diagonal Correction to the Born-Oppenheimer Approximation: Its Effect on the

Singlet-Triplet Splitting of CH₂ and other Molecular Effects. *J. Chem. Phys.* **1986**, *84*, 4481–4484.

(40) Ghigo, G.; Roos, B. O.; Malmqvist, P.-A. A Modified Definition of the Zeroth-Order Hamiltonian in Multiconfigurational Perturbation Theory (CASPT2). *Chem. Phys. Lett.* **2004**, *396*, 142–149.

(41) Truhlar, D. G.; Garrett, B. C.; Klippenstein, S. J. Current Status of Transition-State Theory. *J. Phys. Chem.* **1996**, *100*, 12771–12800.

(42) Werner, H.-J.; Knowles, P. J.; Knizia, G.; Manby, F. R.; Schutz, M.; Celani, P.; Korona, T.; Lindh, R.; Mitrushenkov, A.; Rauhut, G.; et al. *MOLPRO*, version 2012.1, A Package of Ab Initio Programs (<http://www.molpro.net>).

(43) MRCC, a String-Based Quantum chemical program suite; written by M. Kállay, see also Kállay, M.; Surján, P. R. Higher Excitations in Coupled-Cluster Theory. *J. Chem. Phys.* **2001**, *115*, 2945–2954.

(44) Stanton, J. F.; Gauss, J.; Harding, M. E.; Szalay P. G. with contributions from Auer, A. A.; Bartlett, R. J.; Benedikt, U.; Berger, C.; Bernholdt, D. E.; Bomble, Y. J.; et al. and the integral packages *MOLECULE* (Almlöf, J.; Taylor, P. R.), *PROPS* (Taylor, P. R.), *ABACUS* (Helgaker, T.; Jensen, H. J.; Jørgensen, P.; Olsen, J.), and ECP routines by Mitin, A. V.; van Wüllen, C. For the current version, see <http://www.cfour.de>.

(45) Frisch, M. J.; Trucks, G. W.; Schlegel, H. B.; Scuseria, G. E.; Robb, M. A.; Cheeseman, J. R.; Scalmani, G.; Barone, V.; Mennucci, B.; Petersson, G. A.; et al. *Gaussian 09*, revision A.1; Gaussian, Inc.: Wallingford, CT, 2009.

(46) Truhlar, D. G.; Garrett, B. C.; Klippenstein, S. J. Current Status of Transition State Theory. *J. Phys. Chem.* **1996**, *100*, 12771–12800.

(47) Georgievskii, Y.; Klippenstein, S. J. Transition State Theory for Multichannel Addition Reactions: Multifaceted Dividing Surfaces. *J. Phys. Chem. A* **2003**, *107*, 9776–9781.

(48) Georgievskii, Y.; Klippenstein, S. J. Variable Reaction Coordinate Transition State Theory: Analytic Results and Application to the C₂H₃+H → C₂H₄ Reaction. *J. Chem. Phys.* **2003**, *118*, 5442–5455.

(49) Klippenstein, S. J.; Allen, W. D. Variable Reaction Coordinate Direct RRKM Theory. *Ber. Bunsen-Ges.* **1997**, *101*, 423–437.

(50) Klippenstein, S. J. Variational Optimizations in the Rice-Ramsberger-Kassel-Marcus Theory Calculations for Unimolecular Dissociations with No Reverse Barrier. *J. Chem. Phys.* **1992**, *96*, 367–371.

(51) Harding, L. B.; Georgievskii, Y.; Klippenstein, S. J. Predictive Theory for Hydrogen Atom: Hydrocarbon Radical Association Kinetics. *J. Phys. Chem. A* **2005**, *109*, 4646–4656.

(52) Georgievskii, Y.; Miller, J. A.; Burke, M. P.; Klippenstein, S. J. *J. Phys. Chem. A* **2013**, *117*, 12146–12154.

(53) Georgievskii, Y.; Jasper, A. W.; Zádor, J.; Miller, J. A.; Burke, M. P.; Goldsmith, C. F.; Klippenstein, S. J. *PAPER v1*, 2014, available from the authors upon request.

(54) Jasper, A. W.; Miller, J. A. Lennard–Jones Parameters for Combustion and Chemical Kinetics Modeling from Full-Dimensional Intermolecular Potentials. *Combust. Flame* **2014**, *161*, 101–110.

(55) Jasper, A. W.; Oana, C. M.; Miller, J. A. “Third-Body” Collision Efficiencies for Combustion Modeling: Hydrocarbons in Atomic and Diatomic Baths. *Proc. Combust. Inst.* **2015**, *35*, 197–204.

(56) Troe, J. Theory of Thermal Unimolecular Reactions at Low Pressures. I. Solutions of the Master Equation. *J. Chem. Phys.* **1977**, *66*, 4745–4757.

(57) Barker, J. R.; Weston, R. E. Collisional Energy Transfer Probability Densities P(E_J;E'_J) for Monatomics Colliding with Large Molecules. *J. Phys. Chem. A* **2010**, *114*, 10619–10633. Barker, J. R.; Weston, R. E. Correction. *J. Phys. Chem. A* **2012**, *116*, 799.

(58) Jasper, A. W.; Pelzer, K. M.; Miller, J. A.; Kamarchik, E.; Harding, L. B.; Klippenstein, S. J. Predictive A Priori Pressure Dependent Kinetics. *Science* **2014**, *346*, 1212–1215.

(59) Sivaramakrishnan, R.; Su, M.-C.; Michael, J. V.; Klippenstein, S. J.; Harding, L. B.; Ruscic, B. Shock Tube and Theoretical Studies on the Decomposition of Propane: Evidence for a Roaming Radical Channel. *J. Phys. Chem. A* **2011**, *115*, 3366–3379.

(60) Sivaramakrishnan, R.; Su, M.-C.; Michael, J. V.; Klippenstein, S. J.; Harding, L. B.; Ruscic, B. Rate Constants for the Thermal Decomposition of Ethanol and Its Bimolecular Reactions with OH and D: Reflected Shock Tube and Theoretical Studies. *J. Phys. Chem. A* **2010**, *114*, 9425–9439.

(61) Sivaramakrishnan, R.; Michael, J. V.; Klippenstein, S. J. Direct Observation of Roaming Radicals in the Thermal Decomposition of Acetaldehyde. *J. Phys. Chem. A* **2010**, *114*, 755–764.

(62) Sivaramakrishnan, R.; Michael, J. V.; Wagner, A. F.; Dawes, R.; Jasper, A. W.; Klippenstein, S. J.; Harding, L. B.; Georgievskii, Y. *Combust. Flame* **2011**, *158*, 618–632.

(63) Kiefer, J. H.; Santhanam, S.; Srinivasan, N. K.; Tranter, R. S.; Klippenstein, S. J.; Oehlschlaeger, M. A. Dissociation, Relaxation and Incubation in the High-Temperature Pyrolysis of Ethane, and a Successful RRKM Modeling. *Proc. Combust. Inst.* **2005**, *30*, 1129–1135.

(64) Jasper, A. W.; Miller, J. A. Theoretical Unimolecular Kinetics for CH₄ + M → CH₃ + H + M in Eight Baths, M = He, Ne, Ar, Kr, H₂, CO, N₂, and CH₄. *J. Phys. Chem. A* **2011**, *115*, 6438–6455.

(65) Jasper, A. W.; Miller, J. A.; Klippenstein, S. J. Collision Efficiency of Water in the Unimolecular Reaction CH₄ (+H₂O) → CH₃ + H (+H₂O): One-Dimensional and Two-Dimensional Solutions of the Low-Pressure-Limit Master Equation. *J. Phys. Chem. A* **2013**, *117*, 12243–12255.

(66) Jasper, A. W.; Kamarchik, E.; Miller, J. A.; Klippenstein, S. J. First-Principles Binary Diffusion Coefficients for H, H₂, and Four Normal Alkanes + N₂. *J. Chem. Phys.* **2014**, *141*, 124313.

(67) Miller, J. A.; Klippenstein, S. J.; Raffy, C. Solution of Some One- and Two-Dimensional Master Equation Models for Thermal Dissociation: The Dissociation of Methane in the Low-Pressure Limit. *J. Phys. Chem. A* **2002**, *106*, 4904–4913.

(68) Kamarchik, E.; Jasper, A. W. Anharmonic State Counts and Partition Functions for Molecules via Classical Phase Space Integrals in Curvilinear Coordinates. *J. Chem. Phys.* **2013**, *138*, 194109.